Intervalence-Resonant Raman Spectroscopy of Strongly Coupled Mixed-Valence Cluster Dimers of Ruthenium

Reginaldo C. Rocha,[†] Mac G. Brown,[†] Casey H. Londergan,[‡] J. Catherine Salsman,[‡] Clifford P. Kubiak,[‡] and Andrew P. Shreve*,[†]

Bioscience Division, MS G755, Los Alamos National Laboratory, Los Alamos, New Mexico 87545, and Department of Chemistry, University of California, San Diego, La Jolla, California 92093-0358

Received: March 22, 2005; In Final Form: June 20, 2005

Resonance Raman spectroelectrochemistry (RR-SEC) at −20 °C has been performed on the pyrazine-bridged dimer of μ-oxo-centered trinuclear ruthenium−acetate "clusters"− $[(dmap)(CO)(\mu\text{-}OAc)_6(\mu_3\text{-}O)Ru_3(\mu\text{-}L_b)\text{-}Ru_3(\mu_3\text{-}O)(\mu\text{-}OAc)_6(CO)(dmap)]^n$ (where dmap = 4-(dimethylamino)pyridine and L_b = pyrazine-h_4 and pyrazine-d_4)−in three oxidation states: $n = 0, -1$, and -2. In the one-electron reduced, "mixed-valent" state (overall −1 charge and a single odd electron; formal oxidation states [II, II, III]−[III, III, II] on the metal centers), the Raman excitation at 800 nm is resonant with a cluster-to-cluster intervalence charge-transfer (IVCT) band. Under these conditions, scattering enhancement is observed for all four totally symmetric vibrational modes of the bridging pyrazine ligand (ν_{8a}, ν_{9a}, ν_1, and ν_{6a}) in the investigated spectral range (100−2000 cm^{-1}), and there is no evidence of activity in non-totally symmetric vibrations. Resonantly enhanced Raman peaks related to peripheral pyridyl (dmap) ligand modes and low-frequency features arising from the trigonal Ru_3O cluster core and the cluster[Ru]−[N]ligand vibrations were also observed in the spectra of the intermediate-valence ($n = -1$) cluster dimer. The vibrational assignments and interpretations proposed in this work were reinforced by observation of characteristic isotopic frequency shifts accompanying deuteration of the bridging pyrazine. The results reveal that the fully symmetric (A_g) vibrational motions of the organic bridge are coupled to the nominally metal cluster-to-metal cluster fast intramolecular electron transfer (ET) and provide validation of the near-delocalized description according to a predicted three-site/three-state (e.g., metal−bridge−metal) vibronic coupling model, in which the important role of the bridging ligand in mediating electronic communication and delocalization between charge centers is explicitly considered. Further compelling evidence supporting an extended five-state model, which incorporates the peripheral cluster-bound pyridyl ligands, is also presented.

Introduction

A full understanding of electronic coupling and delocalization in molecular mixed-valence systems poised near the localized-to-delocalized transition[1−3] (i.e., at the boundary of the Robin−Day[4] classes II and III) has been recognized as a challenging problem in the context of fast electron-transfer reactions (see, for instance, refs 5−8). A well-known case is the Creutz−Taube ion, $[(NH_3)_5Ru(\mu\text{-}pz)Ru(NH_3)_5]^{5+}$ (where pz = pyrazine).[9−12] For this "mixed-valence" complex, about three decades of experimental and theoretical investigation has been needed to reach some agreement on the delocalized nature of the electronic structure, and some observables still remain to be explained.[1] It is increasingly clear, though, that such systems are often well described by a three-site/three-state vibronic coupling model, as proposed and developed by Ondrechen and co-workers.[13−16] Such models explicitly include electronic and vibrational participation of the bridging ligand in addition to the metal centers. According to this M−L_b−M scheme (L_b = bridging ligand; M = metal site), the so-called metal-to-metal "intervalence" charge transfer (IVCT) transition is actually a symmetry-allowed B → N (bonding → nonbonding) electronic transition, analogous to the allyl-radical π molecular orbital (MO) transition, that would display bridge-to-metal center (i.e., M ← L_b → M) charge-transfer character. The coupling of symmetric bridge-centered and metal−ligand vibrational motions to the nominal IVCT transition is therefore predicted by this three-state vibronic model.

One powerful experimental tool to verify such a vibronic description is resonance Raman spectroscopy[17−19] involving excitation in the IVCT transition. A possible difficulty with this approach, however, is that IVCT bands of most transition-metal dimers bridged by common (*N*-heterocyclic) organic ligands lie in the near-infrared (NIR) or infrared (IR) spectral regions. From the resonance Raman instrumentation standpoint, this introduces experimental difficulties due to a general unavailability of suitable sources or detectors. An approach to avoid these limitations is to seek chemical systems that exhibit higher-energy IVCT transitions. Such a convenient feature has recently been explored[20] in a versatile series of symmetric pyrazine-bridged mixed-valence "dimers of trimers" (Figure 1) of the type $[(L_p)\text{-}(CO)(\mu\text{-}OAc)_6(\mu_3\text{-}O)Ru_3(\mu\text{-}pz)Ru_3(\mu_3\text{-}O)(\mu\text{-}OAc)_6(CO)(L_p)]^-$, where the formal oxidation states on the six Ru ions are [II, II, III]−[III, III, II]. For these complexes, IVCT bands are observed around 800 nm.[5,21] In addition, this system allows tunability of the electronic communication across the pyrazine bridge between the two largely delocalized μ_3-oxo triruthenium moieties (usually called clusters[22]) by variation of the peripheral ligand (L_p). The

* Corresponding author: e-mail shreve@lanl.gov.
[†] Los Alamos National Laboratory.
[‡] University of California, San Diego.

10.1021/jp051482+ CCC: $30.25
Published on Web 09/21/2005

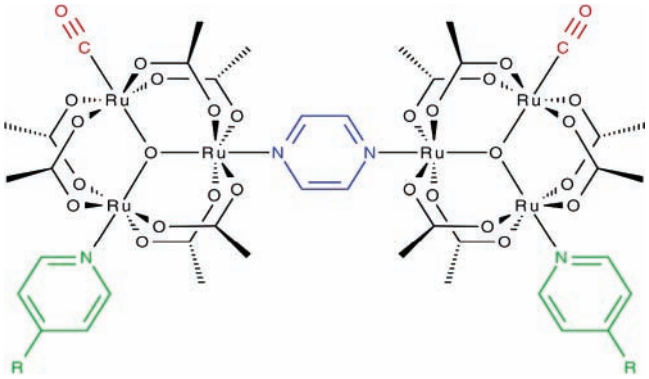

Figure 1. Pyrazine-bridged dimer of trinuclear ruthenium clusters.

dynamic effects of fast ($10^{11}-10^{12}$ s^{-1}) thermal electron transfer on IR vibrational spectra have also been demonstrated by partial coalescence of the cluster-bound carbonyl IR bands.[5,7,21,23,24]

In the particular case of L_p involving a series of pyridyl ligands—that is, 4-(dimethylamino)pyridine (dmap), pyridine (py), and 4-cyanopyridine (cpy)—the magnitude of metal−metal electronic coupling, delocalization, and ET rates vary in the following order of L_p: dmap > py > cpy.[5,21] If pyridine is taken as a reference, the observed order can be rationalized in terms of different degrees of electron-donating (dmap) or -withdrawing (cpy) abilities from the groups on the 4-position of pyridyl, which in turn modulate the energy match between π-type orbital levels of metal clusters and bridging pyrazine.

We recently reported the resonance Raman spectra obtained upon excitation ($\lambda_{exc} = 750$ nm) within the IVCT bands of these three (L_p = dmap, py, cpy) ruthenium "dimers of trimers".[20] These data provided an opportunity to explore how vibronic contributions of specific normal modes vary as electronic communication strength is systematically adjusted near the localized-to-delocalized behavior. With the objective of expanding our previous work, we performed further investigations and describe herein a more comprehensive resonance Raman study of $[(dmap)(CO)(\mu\text{-}OAc)_6(\mu_3\text{-}O)Ru_3(\mu\text{-}pz)Ru_3(\mu_3\text{-}O)(\mu\text{-}OAc)_6(CO)(dmap)]^n$ (**1**^{n}) in three oxidation states: $n = 0$, isovalent oxidized species (**1**^{0}); $n = -1$, "mixed-valent" one-electron-reduced species (**1**$^-$); and $n = -2$, isovalent two-electron-reduced species (**1**$^{2-}$). The generation, in situ, of these redox states was accomplished by means of a spectroelectrochemical (SEC) approach. To improve the stability of the mixed-valent species ($n = -1$) and especially to avoid decomposition of the fully reduced species ($n = -2$), the experiments were run at low temperature (−20 °C) and a variable-temperature thin-layer reflectance SEC cell was used.[25] To provide further support to our assignments and interpretations, the modified version of **1** with deuterated bridging ligand (pyrazine-d_4), **2** (in its three oxidation states **2**^{0}, **2**$^-$, and **2**$^{2-}$), was also investigated in the present work.

The reason this particular member [with L_p = dmap and R = $N(CH_3)_2$ in Figure 1] of the above series of cluster dimers was chosen in this study is 3-fold: (i) it displays the largest electronic delocalization and fastest IVCT dynamics of the series and approaches borderline behavior between localized (class II) and delocalized (class III) properties on the vibrational time scale;[5,7,21] (ii) its large potential separation for the 0/−1 and −1/−2 redox couples, and thus great stability toward comproportionation, makes it easier to (electro)generate the mixed-valent (−1) state by controlled-potential electrolysis in a wide electrochemical potential window;[5,20,21,23] and (iii) the fully reduced (−2) state, which could not be studied in our previous Raman investigation at room temperature, exhibits pronounced stability at temperatures from −30 to −10 °C, as observed and noted elsewhere.[5,21,23]

Experimental Section

Materials and Samples. The preparation and characterization of the neutral cluster dimers **1**^{0} and **2**^{0} have been reported previously by Ito, Kubiak, and co-workers.[5,21] The one-electron-reduced, mixed-valent ($Ru^{II}Ru^{II}Ru^{III}-Ru^{III}Ru^{III}Ru^{II}$) species (**1**$^-$ and **2**$^-$) and the two-electron-reduced, isovalent ($Ru^{II}Ru^{II}Ru^{III}-Ru^{III}Ru^{II}Ru^{II}$) species (**1**$^{2-}$ and **2**$^{2-}$) were generated in situ, in the spectroelectrochemical (SEC) cell. This involved controlled-potential bulk electrolysis of the corresponding neutral (i.e., fully oxidized; $Ru^{II}Ru^{III}Ru^{III}-Ru^{III}Ru^{III}-Ru^{II}$) isolated counterpart at −1.1 and −1.6 V vs SCE, respectively, in methylene chloride solutions containing ca. 1−2 mM sample and 0.1 M n-NBu_4PF_6 (TBAH) as supporting electrolyte. Dry solvent (CH_2Cl_2) and tetra-*n*-butylammonium hexafluorophosphate were purchased commercially (Acros) and used as supplied.

Instrumentation and Methods. Raman spectra were obtained in a backscattering geometry from solution samples in the SEC cell. Raman excitation was carried out at $\lambda_{exc} = 801$ nm from an Ar^+-pumped Ti:sapphire laser (Spectra Physics model 3900) operating at approximately 7−8 mW power. Scattered light was collected and passed through a triple spectrometer (Spex 1877) onto a liquid nitrogen cooled charge-coupled device (CCD) detection system (Princeton Instruments) interfaced to a PC. Typical integration times to acquire spectra were 5−10 min (average of at least 30 scans of 10 s). Data were collected and processed by use of Princeton Instruments WinSpec32 software. Spectra were calibrated with known spectral lines from low-intensity Ne calibration lamps.

In situ controlled-potential electrolyses were performed with a variable-temperature, thin-layer reflectance SEC cell[25] containing a concentric three-electrode system consisting of a 7.5-mm Pt disk working electrode, a Ag ring reference electrode, and a Pt ring counterelectrode. The cell contains a fused-silica window and a 200-μm Teflon spacer. Low-temperature (−20 °C) control was provided by a Neslab external cooling system circulating ethylene glycol. A Bioanalytical Systems model CV-50W potentiostat was employed in all electrochemical measurements. Cyclic voltammetric experiments used a standard three-electrode arrangement in which the working electrode is a Pt disk (o.d. = 1.6 mm), the auxiliary electrode is a coil of Pt wire, and the reference electrode consists of a Ag wire immersed in an acetonitrile solution containing 0.01 M silver nitrate and 0.1 M supporting electrolyte (TBAH). The sample solutions were thoroughly deoxygenated with an argon stream. All potentials reported herein were appropriately converted to give values versus saturated calomel electrode (SCE).

Results

The Raman spectroscopic data were all obtained with excitation wavelength (λ_{exc}) at 801 nm. The monoanionic (−1) and dianionic (−2) species were (electro)generated, in situ, by stepwise reduction of the starting isolated neutral (0) species at −1.1 and −1.6 V vs SCE, respectively. The application of these potentials was based on the half-wave potentials ($E_{1/2}$) determined by cyclic voltammetry as follows: −0.90 and −1.34 V vs SCE for 0/−1 and −1/−2, respectively. The potential separation ($\Delta E_{1/2}$) between the two redox couples is 440 mV, which translates into a comproportionation constant, K_c, of 2.7×10^7. Therefore, there is a wide potential window in which the mixed-valent (−1) species is stable and can be formed by

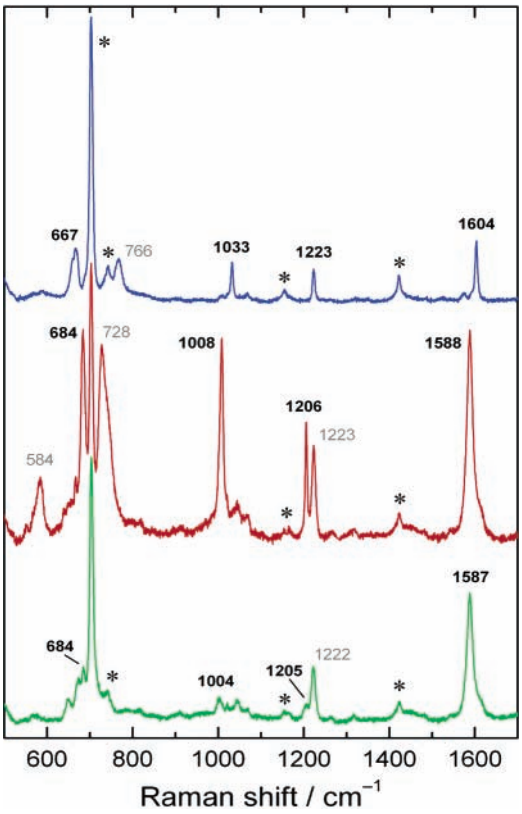

Figure 2. Raman SEC spectra ($\lambda_{exc} = 801$ nm) of $\mathbf{1^0}$ (top, blue; @ 0.0 V), $\mathbf{1}^-$ (middle, red; @ −1.1 V), and $\mathbf{1}^{2-}$ (bottom, green; @ −1.6 V) in CH_2Cl_2/TBAH at −20 °C. Solvent peaks are marked by asterisks, and potentials are versus SCE.

controlled-potential electrolysis without any contamination from the isovalent (0 and −2) species. Both monoelectronic processes were fully reversible in the spectroelectrochemistry, as deduced from the complete spectral recovery of interchangeable redox species.[26]

The Raman spectra of **1** in its three relevant oxidation states (i.e., fully oxidized, mixed-valent, and fully reduced) are shown in Figure 2, and corresponding electronic absorption spectra with λ_{exc} noted are available as Supporting Information Figure SI-1. Except for $\mathbf{2}^-$ (whose spectrum is compared to that of $\mathbf{1}^-$ in Figure 4) the Raman spectra of **2** are not shown herein but are also available as Supporting Information Figure SI-2. Vibrational frequencies for the peaks most relevant to this discussion, including those of **2**, are collected in Table 1. The spectral assignments are grouped according to frequency regions, as presented below.

Region from 1700 to 900 cm^{-1}. In Figure 2 (top), three major peaks can be identified for $\mathbf{1^0}$ in the 1700−900 cm^{-1} range: 1604, 1223, and 1033 cm^{-1}. Upon monoelectronic reduction to give the mixed-valence state ($\mathbf{1}^-$), these peaks undergo significant downshifts to 1588, 1206, and 1008 cm^{-1}, respectively, as shown in Figure 2 (middle); a fourth peak at 1223 cm^{-1} newly appears in $\mathbf{1}^-$, as confirmed in experiments with deuterated pyrazine and discussed below. No substantial shift is observed accompanying further reduction to yield the fully reduced species ($\mathbf{1}^{2-}$), as shown in Figure 2 (bottom). In addition to the frequency shift, a strong intensity enhancement[27] is exhibited in the Raman spectrum of $\mathbf{1}^-$ compared with that of $\mathbf{1^0}$. The same intensification is not observed in the spectrum of $\mathbf{1}^{2-}$. This is not unexpected, since neither of the isovalent species has significant electronic absorption at 801 nm.[5,21,28] The mixed-valent species, on the other hand, displays an absorption band with λ_{max} around 820 nm ($\epsilon_{max} = 12\,200$ M^{-1} cm^{-1}; width = 3760 cm^{-1})—previously attributed to the IVCT (cluster-to-cluster) transition[5,21]—and thus satisfies the condition for resonance Raman scattering intensity enhancement.

The above set of Raman peaks was assigned to three totally symmetric vibrations of the bridging pyrazine (modes ν_{8a}, ν_{9a}, and ν_1; see Figure 3)[29,30] by comparison of the vibrational frequencies for **1** with those for its deuterated counterpart (**2**). As shown in the resonance Raman spectra of Figure 4, for the mixed-valence state of **1** (top) and **2** (bottom), all three of these peaks have their frequencies downshifted (to 1541, 985, and 899 cm^{-1}; $\Delta\tilde{\nu} = 47$, 221, and 109 cm^{-1}, respectively) upon deuteration of the bridging pyrazine ligand. The isotopic frequency shifts from $\mathbf{1}^-$ to $\mathbf{2}^-$ ($\Delta\tilde{\nu}$) are consistent with those observed for free pyrazine,[30] as listed in Table 1.

In addition to the three characteristic peaks originating from totally symmetric vibrational modes of pyrazine in the 1700−900 cm^{-1} region, two remaining unshifted peaks can be observed at 1590 and 1224 cm^{-1} in the spectrum of the deuterated mixed-valent species ($\mathbf{2}^-$), shown in Figure 4 (bottom). Since both peaks also appear in the spectrum of $\mathbf{1}^-$ (Figure 4; top) at similar frequencies—even though the first is clearly overlapped with the pz[ν_{8a}] peak that shifts to 1541 cm^{-1} following deuteration—they may be assigned to the analogous ν_{8a} (ν_{ring}) and ν_{9a} (δ_{C-H}) modes of the peripheral pyridyl (dmap) ligands. The fact that the peak corresponding to the pyrazine ν_{8a} mode is overlapped with that from the pyridyl ν_{ring} vibration in $\mathbf{1}^-$, as demonstrated in this work by isotopic modification of the bridge, also explains the unusual broadness of the resulting convoluted band with maximum intensity at 1588 cm^{-1}, which could not be understood in our previous investigation.[20] Also, note that no Raman peaks from non-totally symmetric modes of either bridging pyrazine or peripheral pyridyl ligands have been observed within this spectral region.

Region from 900 to 500 cm^{-1}. In this region, the peak at 684 cm^{-1} in the spectrum of $\mathbf{1}^-$ (Figure 4, top) is the only one that shifts (to 655 cm^{-1} in $\mathbf{2}^-$) upon deuteration of pyrazine (Figure 4, bottom). Thus, it can be assigned to the totally symmetric ν_{6a} mode[29,30] involving the pz−bridge δ_{ring} vibration (see Figure 3). The corresponding peak in the spectra of the fully reduced species $\mathbf{1}^{2-}$ and $\mathbf{2}^{2-}$ appears at these same frequencies but with lower intensities (Figures 2 and SI-2). Interestingly, and unlike the other three sets of totally symmetric vibrations of pyrazine above, the ν_{6a} mode exhibits lower frequencies in the fully oxidized $\mathbf{1^0}$ and $\mathbf{2^0}$ species—667 and 646 cm^{-1}, respectively—relative to those observed for the reduced species.

Two other peaks at 728 and 584 cm^{-1} remain unshifted from $\mathbf{1}^-$ to $\mathbf{2}^-$ (Figure 4) and were assigned to the B_2 and A_1 components, respectively, of the asymmetric in-plane vibration of the central oxygen (μ_3-oxo bridge); that is, $\nu_{as}(Ru_3O)$ for the individual trigonal cluster moieties in an approximately C_{2v} local symmetry.[31] An assignment of these particular modes has been made previously by Cannon and co-workers[32] for Fe cluster monomers of the type $[Fe^{III}_2Fe^{II}(O)(CH_3COO)_6(L)_3]$ and has also been further exploited in a temperature-dependent IR spectral line shape analysis of the dynamic $Fe^{III}Fe^{III}Fe^{II} \leftrightarrow Fe^{III}$-$Fe^{II}Fe^{III}$ exchange in order to estimate the "intracluster" electron-transfer rate.[33]

This pair of peaks is not evident in the spectra of the reduced and oxidized isovalent species of both **1** (Figure 2) and **2** (Figure SI-2), although a peak at 766 cm^{-1} is present in the spectra of both fully oxidized ($\mathbf{1^0}$ and $\mathbf{2^0}$) species. While the origin of this latter peak for the neutral species is not totally understood at

TABLE 1: Summary of Raman Vibrational (pz) Mode Frequencies for the Pyrazine-Bridged Cluster Dimers and Free Pyrazine[a]

	mode 6a; δ_{ring} $\tilde{\nu}$ (cm^{-1})			mode 1; ν_{ring} $\tilde{\nu}$ (cm^{-1})			mode 9a; δ_{C-H} $\tilde{\nu}$ (cm^{-1})			mode 8a; ν_{ring} $\tilde{\nu}$ (cm^{-1})		
species	pz-h_4	pz-d_4	$\Delta\nu_{6a}$ (cm^{-1})	pz-h_4	pz-d_4	$\Delta\nu_1$ (cm^{-1})	pz-h_4	pz-d_4	$\Delta\nu_{9a}$ (cm^{-1})	pz-h_4	pz-d_4	$\Delta\nu_{8a}$ (cm^{-1})
$\mathbf{1^0/2^0}$	667	646	21	1033			1223	1002	221	1604	1561	43
$\mathbf{1^-/2^-}$	684	655	29	1008	899	109	1206	985	221	1588	1541	47
$\mathbf{1^{2-}/2^{2-}}$	684	655	29	1004	899	105	1205	985	220	1587	1541	46
pz (exp)[b]	596	586	10	1015	883	132	1230	1006	224	1578	1536	42

[a] Mode labels follow Lord's notation (ref 29). [b] Literature values from ref 30.

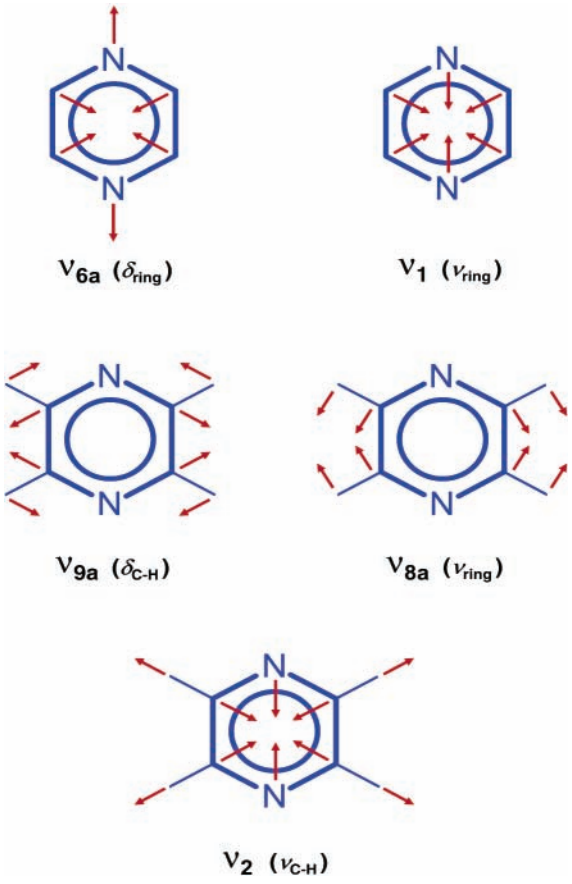

Figure 3. Schematic of totally symmetric (A_g) vibrational normal modes of pyrazine (D_{2h} symmetry).

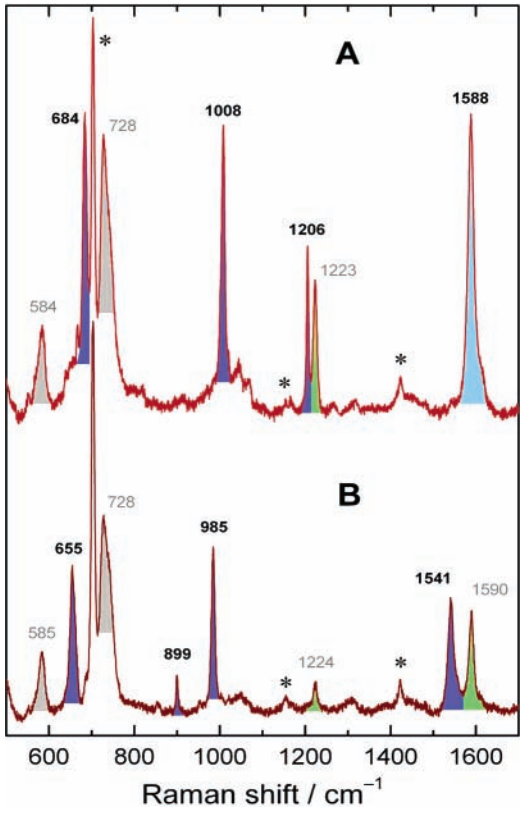

Figure 4. Resonance Raman spectra (λ_{exc} = 801 nm) of the "mixed-valent" $\mathbf{1}^-$ (top) and $\mathbf{2}^-$ (bottom) species, @ −1.1 V vs SCE, in CH_2Cl_2/TBAH at −20 °C. Solvent peaks are marked by asterisks. The shading colors represent the assignments in terms of molecular fragments, as follows: blue, bridging pz; green, peripheral dmap; cyan, bridging pz + peripheral dmap; gray, cluster core Ru_3O. See text for details.

the moment, it is worth noting that both carboxylate and pyridyl groups might also present vibrational modes with typical frequencies around 766 cm^{-1}.[32,34] Density functional theory (DFT) calculations[35] of vibrational frequencies (at the B3LYP[36,37] 6-311++G** level) were performed in this work for the free (uncoordinated) dmap ligand and indicated the presence of a Raman-active symmetric (A_1) vibration at 761 cm^{-1} involving the analogue of the pz[ν_{6a}] mode in a C_{2v} environment for dmap.

Region from 500 to 100 cm^{-1}. A low-intensity peak can be observed for the mixed-valent species in the low-frequency region, at ca. 210 cm^{-1} (Figure 5), and was tentatively assigned to the symmetric metal−heterocyclic ligand (ν_{Ru-N}) stretch. This vibrational mode has previously been observed at similar frequencies for a series of symmetric cluster monomers of the type $[M_3(O)(OOCR)_6(L)_3]$.[32,34] For the specific Ru clusters studied here, it has also been anticipated to exist near the above observed frequency on the basis of DFT calculations.[24]

The additional weak feature that appears at ca. 315 cm^{-1} is most likely associated with the $\nu_{sym}(Ru-O; A_{1g})$ vibration involving some of the three equatorial RuO_4 (metal−carboxylate) framework in a local square-planar (D_{4h}) environment,[32,34] although the out-of-plane $\delta_{sym}(Ru_3O)$ vibration involving the planar trigonal core may also display similar frequencies (at least for the D_{3h} microsymmetry[34]).

Discussion

Of the five totally symmetric (A_g) vibrations of pyrazine[29,30,38] depicted in Figure 3, four (ν_{8a}, ν_{9a}, ν_1, and ν_{6a}) were observed in the Raman spectra of **1** and **2**. All four have enhanced scattering intensities[27] in the mixed-valence ($n = -1$) state when the Raman excitation line (801 nm) is resonant with the so-called IVCT electronic transition (see Supporting Information Figure SI-1). The fifth mode (ν_2) involves the C−H stretches and lies too high in frequency (~3050 cm^{-1} for the free, uncoordinated ligand[29,30]) to be investigated by our approach. However, it is not expected to significantly couple to changes in redox states and should have only a minor role in mediating the electronic interaction between coordinated clusters. In contrast, spectroscopic observations detailed below reveal that

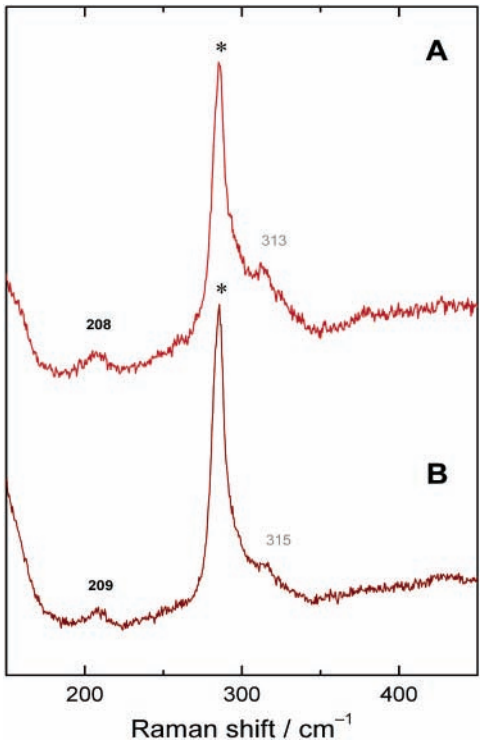

Figure 5. Raman spectra (λ_{exc} = 801 nm) of the "mixed-valent" $\mathbf{1}^-$ (top) and $\mathbf{2}^-$ (bottom) species, @ −1.1 V vs SCE, in CH_2Cl_2/TBAH at −20 °C. Solvent peaks are marked by asterisks.

the other modes discussed are all vibronic participants in electronic delocalization in the ruthenium "dimers of trimers". Unlike the Creutz−Taube ion, for which activity in both totally and non-totally symmetric pz modes has been reported[39] on the basis of Raman spectra excited postresonance (λ_{exc} = 1320 nm) with the NIR absorption (λ_{max} = 1570 nm), no Raman peaks from non-totally symmetric modes of the bridging pyrazine have been observed for the cluster dimers.

The fact that three (ν_{8a}, ν_{9a}, and ν_1) of the four resonance Raman-enhanced totally symmetric bridging modes shift to lower frequency upon monoelectronic reduction from the isolated (0) state is indicative of partial electronic occupation in the pyrazine π^* orbital in the (−1) oxidation state and suggests that electronic occupation on pyrazine is an important contributor to the electronic character of the mixed-valence state. The fact that the ν_{6a} mode follows an opposite trend and shifts to higher frequency in going from neutral to reduced species is not fully understood yet, and molecular modeling is underway to clarify this point. However, it is worth noting that, of the totally symmetric pz modes, ν_{6a} is the only one to involve mostly the two nitrogen-coordinating atoms. Consequently, its frequency is expected to be especially sensitive to the metal coordination. A relevant observation is that, of these modes, ν_{6a} has by far the largest relative shift in frequency when free pyrazine and metal-coordinated pyrazine are compared (see Table 1). Therefore, frequency changes in ν_{6a} may be dominated by coordination effects rather than by electronic effects within the pyrazine. The other totally symmetric modes, in contrast, involve mostly C−C and C−H vibrations and therefore are significantly less sensitive to coordination effects, as can be deduced from a direct comparison of normal-mode frequencies in Table 1 for coordinated versus uncoordinated pyrazine.

Overall, the above observations suggest that there are both softening of bridge vibrations and increases in metal−pyrazine interactions in the reduced species. These effects are consistent with population of an orbital that is substantially delocalized

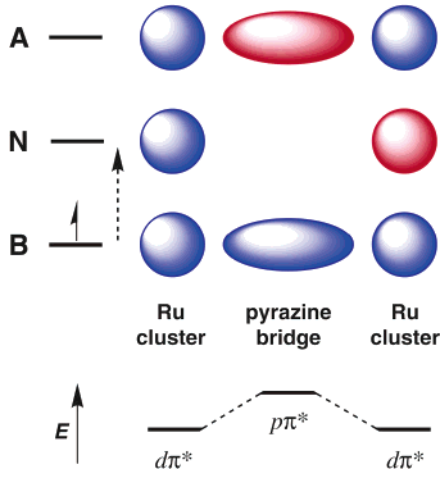

Figure 6. Qualitative MO diagram illustrating the three-level (bonding, nonbonding, and antibonding) combinations from the three-center model. Electronic occupation is shown for the mixed-valence (−1) state, and the electronic transition allowed by symmetry is indicated by a dashed arrow.

over the entire molecule and that has antibonding character on the pyrazine but bonding interactions between the pyrazine and metal ions. Such an orbital is the highest occupied molecular orbital (HOMO) in the −1 and −2 states within a delocalized picture, as discussed below. While changes in local symmetry due to charge localization could also influence the vibrational character and frequency of ν_{6a}, these are expected to be less significant in systems close to the class II/III boundary, an observation also consistent with the dominance of totally symmetric modes in the Raman spectra from all oxidation states. Finally, we note that, for all modes, comparison of frequency shifts involved in moving from −1 to −2 states may be additionally complicated by factors such as electron correlation effects, also discussed further below.

There is clear evidence for the totally symmetric modes of pyrazine being enhanced in resonance Raman in the (−1) state relative to the neutral state due to their coupling to the IVCT transition. Coupling of such bridging ligand modes to the charge-transfer process is consistent with the predictions of a three-center/three-state model,[40] as originally proposed by Ondrechen and co-workers.[13−16] Although quantitative application of this model to the charge-transfer system reported here would require additional effort, particularly in developing a treatment of the role of solvent in mediating charge-transfer dynamics,[23] it provides a useful qualitative framework for interpreting experimental results. In this description, the "intervalence" transition (which is conventionally thought of as a direct metal-to-metal charge transfer involving two centers/two states in the context of the semiclassical Marcus−Hush formalism[41,42]) is rather represented by a symmetry-allowed B → N electronic excitation from a bonding level (B) to a nonbonding level (N), as illustrated in Figure 6. The B and N states are two of the "three states" [with the third being antibonding (A)] that originate from the combination of the MOs with involvement of all the three "centers", namely, the two cluster units plus the intermediate ligand that connects them (see Figure 6). Because the nonbonding electronic level has a node on the bridging ligand, the B → N electronic transition has the character of a pyrazine-to-clusters charge-transfer transition, that is, a ligand-to-metals charge transfer. Such a transition is expected to involve significant nuclear displacement along the symmetric normal coordinates of the bridge due to the strengthening of its bonds associated with depletion of electron density in the pyrazine π^* orbital.

Thus, the totally symmetric vibrations of pyrazine (as well as the symmetric cluster−pyrazine combination mode) should be vibronically coupled to the B → N electronic transition, as experimentally confirmed herein.

As pointed out and discussed by Londergan and Kubiak,[24] the relative simplicity of the above Hückel-type model has been questioned in the case of the Creutz−Taube ion,[16] partially due to anticipated problems with near-degenerate metal $d\pi$ orbitals on each Ru ion and the possibility of spin−orbit coupling interactions. However, results of DFT calculations for a "monomeric" trinuclear cluster[24] suggest that a model invoking only three electronic states (electronic occupation in a single molecular orbital on each cluster moiety and in a single orbital on the bridging pyrazine ligand) should be reasonably valid in the case of the cluster dimer presented here. According to a qualitative MO scheme proposed for these trinuclear clusters,[24] only one cluster orbital (the delocalized antibonding MO) should have a significant exchange coupling interaction with the bridging ligand's low-lying π^* level, reflecting the small energy gap and efficient spatial overlap between the cluster HOMO and the π^* lowest unoccupied molecular orbital of pyrazine. Hence, in a simple picture and for the purposes of the three-state model, the mixed-valence (−1) state of the cluster dimer can be viewed in terms of a single electron exchanging between three states: two with the electron in cluster-based $d\pi^*$ orbitals and one with the electron in the higher energy π^* orbital of the bridging pyrazine ligand (see Figure 6). In this way, a single-electron Hückel Hamiltonian is expected to adequately reflect the electronic properties of this particular three-site system, in its mixed-valent (−1) form, without the need for invoking higher levels of theory.[43] However, we note that, even in this system, properties of the fully reduced (−2) species would be influenced by electron correlation effects. This could account for the apparent lack of additional electron density on the pyrazine bridge in passing from the mixed-valence to the fully reduced state, as indicated by the significant saturation in frequency shifts of the pyrazine vibrations at the −1/−2 reduction step.

It has recently been suggested[24] that although the three-site (cluster−L_b−cluster) picture of Figure 6 suffices to explain the "mixed-valency" and related spectroscopic observables of these cluster dimers, a *five*-center model with additional incorporation of the peripheral pyridyl ligands (see Figure 7) might provide a more accurate vibronic description.[44] Specifically, the existence of an additional low-energy band in the NIR region ($\lambda_{max} \sim 1500$ nm)[5,21,28] provides plausible evidence for the lowest-energy (B → N_1) electronic transition among the three B → N transitions in the five-state scheme (Figure 7). The above-explored "IVCT" absorption band at ca. 800 nm would, in this case, correspond to the higher-energy (B → N_3) transition, while the intermediate B → N_2 electronic transition is not symmetry-allowed. Further theoretical insight corroborating this idea comes from density functional MO calculations on model cluster monomers[24] pointing toward substantial cluster−L_p coupling. The pyridyl group features available low-lying π^* orbitals that can effectively interact with the cluster (metal-centered) $d\pi^*$ orbital, although the overlap is less energetically favorable than for pyrazine.

Spectroscopic validation of this more detailed five-center/five-state scheme requires information that could not be provided by our previous resonance Raman study,[20] in which detailed spectral comparison with the species containing deuterated ligands was not available. Since pyrazine and pyridyl rings have almost coincidental mode frequencies, lack of such comparison imposes a major limitation in unambiguously assigning and discriminating pyrazine versus pyridyl modes as potentially simultaneous contributors to resonance-enhanced Raman vibrational bands. The current spectral attribution on the basis of frequency shifts accompanying deuteration of the pz bridge clearly reveals at least two dmap vibrations in the Raman spectra of $\mathbf{1}^-$ and $\mathbf{2}^-$. Further, by comparison to solvent intensities, these vibrations are resonantly enhanced in the mixed-valence state. Thus, the direct vibronic involvement of the peripheral ligand in the "intervalence" electronic transition is confirmed. Additional evidence that supports this extended multistate model is the fact that vibrational modes involving both the μ-oxo-bridged trinuclear cluster core (i.e., Ru_3O) and the metal cluster−ligand framework (i.e., Ru−N_{ring}) are observed in the resonance Raman spectra of $\mathbf{1}^-$ and $\mathbf{2}^-$. This is a clear indication that molecular fragments from all over the dimeric system ($L_{peripheral}$−M_{core}−$L_{bridging}$−M_{core}−$L_{peripheral}$) are coupled to the "intervalence" charge transfer within the −1 species. Overall, the idea inherent in the pictorial model of Figure 7, in which the ground state is largely delocalized over all five components (i.e., two metal clusters, one bridging ligand, and two peripheral ligands), seems to be fully supported by the experimental findings discussed herein, indicating the appropriateness of a five-state vibronic description.

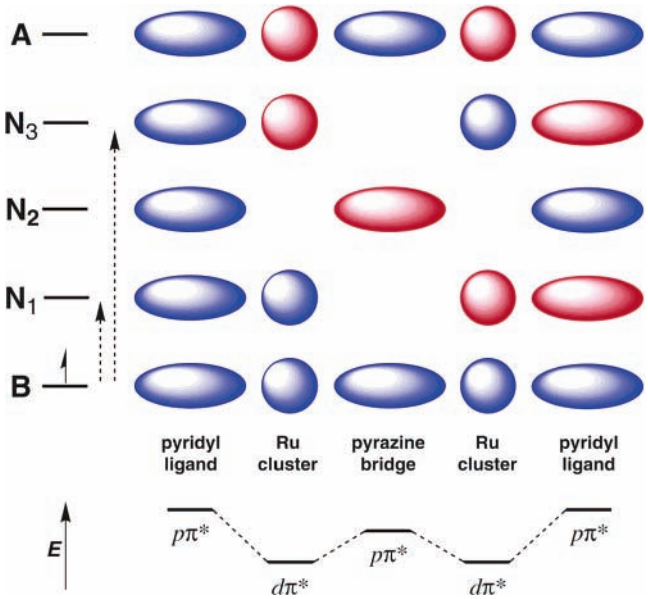

Figure 7. Qualitative MO diagram illustrating the resulting five-level combinations from the five-center model. Electronic occupation is shown for the mixed-valence (−1) state, and the symmetry-allowed electronic transitions are indicated by dashed arrows.[44]

Conclusions

The usefulness of intervalence-resonant Raman spectroscopy in exploring the localized-to-delocalized transition in mixed-valence chemistry is demonstrated in this study. The results presented provide evidence for vibronic coupling of totally symmetric bridging vibrations of pyrazine to the "intervalence" charge transfer, which confirms a near-delocalized description for the mixed-valence cluster dimer. To take into consideration the explicit participation of the peripheral ligands, as also experimentally shown to be vibronically coupled to the "IVCT" process for the intermediate-valence species, a five-center model that should provide a more realistic description of the system is further explored as an extension of the previously proposed three-center/three-state model. Although the important participation of the bridge in mediating electronic communication and

delocalization between charge sites has been discussed here to account for spectroscopic observables in the specific context of these strongly coupled pyrazine-bridged dimers of trinuclear ruthenium complexes, the conclusions should also be broadly applicable and are expected to shed light on general dynamic electron-transfer phenomena and "mixed-valency" behavior of other near-delocalized charge-transfer systems.

Acknowledgment. The support by the Laboratory Directed Research & Development program (LDRD; for the research at LANL) and National Science Foundation (CHE-0315593; for the research at UCSD) is gratefully acknowledged.

Supporting Information Available: Electronic absorption spectra of **1** in all the three oxidation states ($\mathbf{1^0}$, $\mathbf{1^-}$, and $\mathbf{1^{2-}}$), with Raman excitation frequency noted. Raman SEC spectra of **2** in all the three oxidation states ($\mathbf{2^0}$, $\mathbf{2^-}$, and $\mathbf{2^{2-}}$). This material is available free of charge via the Internet at http://pubs.acs.org.

References and Notes

(1) Demadis, K. D.; Hartshorn, C. M.; Meyer, T. J. *Chem. Rev.* **2001**, *101*, 2655.
(2) Brunschwig, B. S.; Creutz, C.; Sutin, N. *Chem. Soc. Rev.* **2002**, *31*, 168.
(3) Nelsen, S. F. *Chem. Eur. J.* **2000**, *6*, 581.
(4) Robin, M. B.; Day, P. *Adv. Inorg. Chem. Radiochem.* **1967**, *10*, 247.
(5) Ito, T.; Hamaguchi, T.; Nagino, H.; Yamaguchi, T.; Washington, J.; Kubiak, C. P. *Science* **1997**, *277*, 660.
(6) Demadis, K. D.; Neyhart, G. A.; Kober, E. M.; White, P. S.; Meyer, T. J. *Inorg. Chem.* **1999**, *38*, 5948.
(7) Londergan, C. H.; Kubiak, C. P. *Chem. Eur. J.* **2003**, *9*, 5963.
(8) Rocha, R. C.; Shreve, A. P. *Inorg. Chem.* **2004**, *43*, 2231.
(9) Creutz, C.; Taube, H. *J. Am. Chem. Soc.* **1969**, *91*, 3988.
(10) Creutz, C.; Taube, H. *J. Am. Chem. Soc.* **1973**, *95*, 1086.
(11) Creutz, C. *Prog. Inorg. Chem.* **1983**, *30*, 1.
(12) Hupp, J. T. In *Comprehensive Coordination Chemistry II*; McCleverty, J. A., Meyer, T. J., Eds.; Elsevier: Amsterdam, 2004; Vol. 2 (Lever, A. B. P., Ed.), p 709.
(13) Zhang, L. T.; Ko, J.; Ondrechen, M. J. *J. Am. Chem. Soc.* **1987**, *109*, 1666.
(14) Ondrechen, M. J.; Ko, J.; Zhang, L. T. *J. Am. Chem. Soc.* **1987**, *109*, 1672.
(15) Zhang, L. T.; Ko, J. J.; Ondrechen, M. J. *J. Phys. Chem.* **1989**, *93*, 3030.
(16) Ferretti, A.; Lami, A.; Ondrechen, M. J.; Villani, G. *J. Phys. Chem.* **1995**, *99*, 10484.
(17) Clark, R. J. H.; Dines, T. J. *Angew. Chem., Int. Ed.* **1986**, *25*, 131.
(18) Myers, A. B. *Chem. Rev.* **1996**, *96*, 911.
(19) Hupp, J. T.; Williams, R. D. *Acc. Chem. Res.* **2001**, *34*, 808.
(20) Londergan, C. H.; Rocha, R. C.; Brown, M. G.; Shreve, A. P.; Kubiak, C. P. *J. Am. Chem. Soc.* **2003**, *125*, 13912.
(21) Ito, T.; Hamaguchi, T.; Nagino, H.; Yamaguchi, T.; Kido, H.; Zavarine, I. S.; Richmond, T.; Washington, J.; Kubiak, C. P. *J. Am. Chem. Soc.* **1999**, *121*, 4625.
(22) Toma, H. E.; Araki, K.; Alexiou, A. D. P.; Nikolaou, S.; Dovidauskas, S. *Coord. Chem. Rev.* **2001**, *219*, 187 and references therein.
(23) Londergan, C. H.; Salsman, J. C.; Ronco, S.; Dolkas, L. M.; Kubiak, C. P. *J. Am. Chem. Soc.* **2002**, *124*, 6236.
(24) Londergan, C. H.; Kubiak, C. P. *J. Phys. Chem. A* **2003**, *107*, 9301.
(25) Zavarine, I. S.; Kubiak, C. P. *J. Electroanal. Chem.* **2001**, *495*, 106.
(26) It is also possible to visually follow the interconversion between redox species in the SEC cell since they display distinct colors in methylene chloride solutions, as follows: 0 = dark blue; −1 = red; −2 = light green.
(27) The comparison of relative peak intensities was based on the solvent peaks.
(28) See also material available as Supporting Information.
(29) Lord, R. C.; Marston, A. L.; Miller, F. A. *Spectrochim. Acta* **1957**, *9*, 113.
(30) Simmons, J. D.; Innes, K. K.; Begun, G. M. *J. Mol. Spectrosc.* **1964**, *14*, 190.
(31) The fact that these two components appear with distinct vibrational frequencies implies some degree of localization of the individual oxidation states on the three ruthenium ions within each cluster moiety. The nominally localized oxidation states for the mixed-valent cluster dimer would be Ru^{III}-$Ru^{III}Ru^{II}$ on one of the cluster moieties and $Ru^{III}Ru^{II}Ru^{II}$ on the other moiety. The higher-frequency (B_2) component is expected to have more character of a $Ru^{III-}O$ stretch, while a more pronounced $Ru^{II-}O$ character would conversely be exhibited by the lower-frequency (A_1) component (see ref 32).
(32) Meesuk, L.; Jayasooriya, U. A.; Cannon, R. D. *J. Am. Chem. Soc.* **1987**, *109*, 2009.
(33) Wu, R. W.; Koske, S. K. A.; White, R. P.; Anson, C. E.; Jayasooriya, U. A.; Cannon, R. D. *J. Chem. Soc., Chem. Commun.* **1994**, 1657.
(34) Johnson, M. K.; Powell, D. B.; Cannon, R. D. *Spectrochim. Acta A* **1981**, *37*, 995.
(35) Frisch, M. J., et al. *Gaussian 03*, Revision B.05; Gaussian, Inc.: Pittsburgh, PA, 2003.
(36) Becke, A. D. *J. Chem. Phys.* **1993**, *98*, 5648.
(37) Lee, C.; Yang, W.; Parr, R. G. *Phys. Rev. B* **1988**, *37*, 785.
(38) These vibrational modes were labeled as by Lord et al. (ref 29), following the original Wilson notation for benzene-like rings: Wilson, E. B. *Phys. Rev.* **1934**, *45*, 706.
(39) Lu, H.; Petrov, V.; Hupp, J. T. *Chem. Phys. Lett.* **1995**, *235*, 521.
(40) The terms three-state and three-center (or three-site) are interchangeably used because the three states B, N, and A arise from the combination of the three MOs on the three centers (or three sites), which in this case are cluster−pz−cluster.
(41) Hush, N. S. *Prog. Inorg. Chem.* **1967**, *8*, 391.
(42) Sutin, N. *Prog. Inorg. Chem.* **1983**, *30*, 441.
(43) It is worth noting that this single-electron occupation differs from the electronic occupation in the three-state model applied to the Creutz−Taube ion. For the Creutz−Taube case, there are a total of three electrons, one from the highest semioccupied $d\pi$ level on the formally $Ru^{3+}/d\pi^5$ moiety and two from the highest fully occupied $d\pi$ level on the formally $Ru^{2+}/d\pi^6$ moiety, in the three MOs of interest. Therefore, for best accuracy, the Creutz−Taube ion must be treated by use of a more sophisticated Hubbard model that includes the energetic effects of electron correlation (see ref 16).
(44) Note that the orbitals resulting from the Hückel-type linear combination in the five-state model are reminiscent of the MOs of the pentadienyl radical in the same way the ones in the three-state model resemble those of the allyl radical. In this sense, the labeling for the five-state model in Figure 7 (i.e., B, N1, N2, N3, and A) is only intended to make the parallel with the corresponding three-state model in Figure 6 more explicit (i.e., N1 and N3 would result from the "split" of the single N level in the original three-state model into "symmetric" and "antisymmetric" combinations), even though we recognize that N1 and N3 have bonding and antibonding character, respectively, with respect to the interaction between clusters and peripheral pyridyl ligands.